Published in final edited form as:
Sci Transl Med. 2010 October 20; 2(54): 54ra77. doi:10.1126/scitranslmed.3001338.

An integrated genomic and pharmacoepigenomic approach predicts therapeutic response of zebularine in human liver cancer*

Jesper B. Andersen, **Valentina M. Factor**, **Jens U. Marquardt**, **Chiara Raggi**, **Yun-Han Lee**, **Daekwan Seo**, **Elizabeth A. Conner**, and **Snorri S. Thorgeirsson**#
Laboratory of Experimental Carcinogenesis, Center for Cancer Research, National Cancer Institute, National Institutes of Health, Bethesda, Maryland 20892-4262, USA

Abstract

Epigenomic changes such as aberrant hypermethylation and subsequent atypical gene silencing are characteristic features of human cancer. Here, we report a comprehensive characterization of epigenomic modulation caused by zebularine, an effective DNA methylation inhibitor, in human liver cancer. Using transcriptomic and epigenomic profiling, we identified a zebularine signature that classified liver cancer cell lines into two major subtypes with different drug-responses. In drug-sensitive cell lines, zebularine caused inhibition of proliferation coupled with increased apoptosis, whereas drug-resistant cell lines were associated with upregulation of oncogenic networks (e.g. *E2F1*, *MYC*, and *TNF*) driving liver cancer growth *in vitro* and in preclinical mouse models. Assessment of zebularine-based therapy in xenograft mouse models demonstrated potent therapeutic effects against tumors established from zebularine-sensitive but not zebularine-resistant liver cancer cells leading to increased survival and decreased pulmonary metastasis. Integration of zebularine gene expression and demethylation response signatures differentiated patients with HCC according to their survival and disease recurrence and identified a subclass of patients within the poor survivors likely to benefit from therapeutic agents that target the cancer epigenome.

INTRODUCTION

Hepatocellular carcinoma (HCC) in adults is the major primary liver cancer and a cause of disability and death worldwide, responsible for over 598,000 deaths yearly(1). Despite the recent success of sorafenib(2–3), a systemic multi-tyrosine kinase inhibitor, only 30% of patients with advanced HCC and liver cirrhosis (Child-Pugh A) are eligible for curative therapy (4), leaving a large group of patients without therapeutic options.

Currently, much effort is dedicated to understanding the molecular pathogenesis of human cancer, developing robust genomic classification, and establishing a prognostic model for survival and treatment options by integrating genomic data with clinical and pathological information(5–9). It is accepted that complementary effects of genetic and epigenetic changes are driving the development of tumors from premalignant lesions to end-stage

#Address requests for reprints to: Snorri S. Thorgeirsson, MD, PhD, National Cancer Institute, Building 37, Room 4146A, 37 Convent Drive, Bethesda, Maryland 20892-4262. snorri_thorgeirsson@nih.gov; fax: (301) 496-0734.

disease(10–11). Our recent analysis of gene expression and promoter CpG island hypermethylation in HCC revealed that both genetic and epigenetic changes contribute to the initiation and progression of liver cancer and correlate with poor survival(12). Epigenetic changes are pharmacologically reversible, offering a promising multi-target translational strategy against cancer in which expression of a variety of silenced genes could be reactivated. In particular, inhibition of DNA methyltransferase 1 (DNMT1), a key enzyme responsible for sustaining the epigenetic profile in normal proliferating cells(13), can reactivate epigenetically silenced tumor suppressor genes and decrease tumor cell growth *in vitro* and *in vivo* by inducing differentiation, apoptosis, and increased immune surveillance(14–15). Thus far, three (DNMT)-inhibiting cytosine nucleoside analogs, 5'-azacitidine, decitabine and zebularine, have been studied as potential anti-cancer drugs(16–18). Decitabine and its prodrug 5'-azacitidine are effective in treatment of various cancers(19–20) and have become incorporated into the clinical management of certain types of hematological malignancies, such as myelodysplastic syndromes (MDS) and acute myeloid leukemia (AML).

Zebularine is a second-generation, highly stable hydrophilic inhibitor of DNA methylation with oral bioavailability, which preferentially targets cancer cells as demonstrated in bladder, prostate, lung, colon, and pancreatic carcinoma cell lines(21), and exhibits low toxicity in mice even after prolonged administration(22–24), possibly as a result of slow conversion of zebularine by ribonucleotide reductase(25). Although aza-nucleoside analogs are effective in treating various cancers(19–20), the formation of irreversible covalent adducts with DNA may cause long-term side effects including DNA mutagenesis, a potential cause of tumor recurrence. In contrast, zebularine forms reversible "wobbling" Watson-Crick base-pair hydrogen bonds with guanidine and adenosine, which significantly reduces the mutagenic rate during DNA replication(26). Given that aberrant methylation is a major event in early and late stages of tumorigenesis(10,27), including hepatocarcinogenesis(12), this process may represent a critical target for cancer risk assessment, treatment, and chemoprevention. Here, we investigated the potential therapeutic efficacy of zebularine against primary human liver cancer. We identified zebularine response gene expression and demethylation signatures which can predict therapeutic response of HCC patients to epigenomic therapy.

RESULTS

DNA CpG methylation predicts survival of HCC patients

Our previous transcriptomic profiling of human HCC revealed the existence of two distinct HCC subtypes A and B that were strongly associated with clinical outcome(5). Patients with subtype A HCC had the worst clinical prognosis (shorter survival and high recurrence). To evaluate the epigenetic profiles these two HCC subtypes, we measured the level of DNA methylation of 807 cancer-related genes in a group of 23 primary HCCs. Multivariate permutation tests showed a higher degree of CpG methylation in subtype A HCCs (figs. S1A, B). Using a 17% change in methylation as a threshold for selection ($\Delta\beta \geq 0.17$, $P<.05$) (28–29), we identified 32 hypermethylated genes that successfully separated the 23 primary HCC samples according to their subtype, suggesting a correlation between clinical outcome and methylation (HR=2.23, 1.0 to 5.5). Bayesian compound covariate prediction modeling confirmed that the genes identified by DNA methylation were characteristic of the HCC survival type with an estimated correlation of 0.96 ($P<.0001$) between methylation profiling and correct subtype classification of the samples. Applying the prediction model to a gene expression data set obtained from 53 primary HCCs(30) demonstrated the ability of the 32 genes identified by methylation profiling to correctly (0.95, $P<.0001$) subclassify an independent group of HCCs by using leave-one out cross-validation (fig. S1C). These 32 genes have known associations with canonical pathways, such as hypoxia, MAPK signaling,

and regulation of apoptosis (*CREB1, DDIT3, EPHX1, PLG, PTHR1*), cellular defense and immune response (*AGXT, CSF3R, EPO, ST6GAL1, TMEFF1, UGT1A1*). This suggests that patients with advanced HCC and tumor hypermethylation may benefit from epigenetic therapy. The data corroborate our previous findings which showed an inverse correlation between the methylation index and length of patient's survival in a cohort of 60 HCC patients with poor (subtype A) and better (subtype B) survival(12).

Establishment of zebularine response signature in liver cancer cell lines

To generate a zebularine response gene signature, we combined the cytotoxic response of zebularine *in vitro* with gene expression profiling. Ten cell lines representing the diversity of primary human liver cancer and displaying differential sensitivity to zebularine treatment were selected for analysis (Fig. 1A and fig. S2A–E). Gene lists of significantly differentially expressed genes were identified at $P \leq .001$ for each cell line and its corresponding untreated control. The common zebularine response gene signature included 323 differentially expressed genes across all treated cell lines. Depending on the response to zebularine *in vitro*, these cell lines were classified either as sensitive or resistant (Fig. 1A and fig. S2A–E). Class comparison using multiple prediction models confirmed the correct classification of the differential response of liver cancer cell lines to zebularine with accuracy ranging within 70% to 95% (table S1A, B). To corroborate the differential drug response in primary cells, we analyzed the effect of zebularine on three early passages primary HCC cell lines (fig. S3). Consistent with our findings in the established liver cell lines, zebularine treatment affected the primary HCC in a drug-sensitive or resistance manner.

More than 95% (308/323) of the genes in the zebularine response gene signature contained at least 1 and less than 8 promoter CpG islands as determined by two independent CpG prediction algorithms(31–32) (CpG content >55%, an observed versus expected CpG dinucleotide density above 0.65, and minimum length 500 bp). This represents an enrichment of CpG island-containing promoters as the genome-wide average is 55 to 60%, suggesting that gene expression changes induced by zebularine may be associated with CpG island methylation. To substantiate the association between the zebularine response gene signature and changes in DNA methylation, we applied methylation-specific arrays to four liver cancer cell lines, two sensitive and two resistant to zebularine (Fig. 1B and figs. S2, S4). Consistent with our transcriptomic profiling (Fig. 1A), the complete demethylation signature distinguished the cell lines according to their zebularine-sensitivity (Fig 1B). The signature included 133 genes with significantly ($P \leq .01$) demethylated CpG loci (more than 17% decrease in methylation ($\Delta\beta$)(29)) as compared to the matched untreated control (table S2). The zebularine sensitive cell lines (Huh7, KMCH) showed preferential demethylation of genes for tumor-suppression, apoptosis, and cell-cycle regulation, whereas the resistant lines (WRL68, WITT) showed a decrease in methylation of tumor-promoting genes (table S2). To validate the demethylation signature, the same cell lines were profiled by HumanMethylation27 beadchips (fig. S5). Hierarchical clustering grouped the cell lines according to their drug-sensitivity, and comparison of the two data sets showed a correlation of 0.7 to 0.8 for each cell line. Despite limited gene-to-gene overlap between zebularine demethylation and gene response signatures, each of these signatures consistently predicted drug response.

Zebularine functions by depleting the cellular DNMT1 activity causing global hypomethylation(21), growth arrest, and reactivation of tumor-suppressor genes. The differential drug-sensitivity was unrelated to the ability of zebularine to inhibit its primary target DNMT1, suggesting that the effect of zebularine on DNA methylation is downstream of DNMT1 (fig. S6). Likewise, induction of cell cycle inhibitor *CDKN1A* which mediates the p53-regulated cell cycle arrest in response to DNA damage was independent of drug effects (fig. S7C). Furthermore, gene set enrichment analysis using curated gene lists for p53

signaling and DNA damage response retrieved from the molecular signatures database (MSigDB) showed no enrichment in expression profiles associated with zebularine sensitivity or resistance making it unlikely that the differential response to zebularine could be attributed to DNA damage (fig. S7A, B).The latter is important because zebularine is a DNA damaging agent and has been previously shown to induce growth inhibition through *CDKN1A* upregulation specific only to cancer cells(21).

The relationship between zebularine response and deregulation of oncogenic pathways

The clear division between zebularine sensitive and resistant cell lines revealed by hierarchical clustering (Figs. 1A, B) points to the existence of distinct molecular subtypes of liver cancer. Analysis of functional connectivity indicated that many of the differentially expressed genes in zebularine sensitive cell lines were known regulators of G2/M progression, including *CCNA2*, *RASSF1*, *AURKA, CDCA8, FANCD2, MDC1, LGACS1, PLAC8*, and *POLB*. Zebularine also affected expression of *CDC2*, a key cell cycle regulatory switch essential for G1/S and G2/M transitions, as well as G1/S checkpoint genes *CCND3, CDKN1B, CDC6, CDC7, CDKN3, DARS, NASP*, and *FOXO4*. Gene expression data correlated well with the aberrant kinetics of cell cycle progression (figs. S2D, E). This result was consistent with the reduced growth rate and higher frequency of apoptosis in the zebularine sensitive as compared to zebularine resistant cells (figs. S2A–C and S8).

To further characterize the mechanisms of resistance, we selected genes that were unique to each group using supervised clustering followed by network analysis. The resistant cell lines demonstrated an upregulation of key regulatory genes involved in cancer progression including *TNF, MYC, CEBPA, MET*, and *EGFR* and down-regulation of two important tumor suppressor networks (VHL and CDKN2A). Overrepresentation of *E2F1* as a core regulator of four key networks (TNF, MYC, VHL, and CDKN2A) suggests that their activation may be critical for the development of zebularine-resistance (figs. S8A–C). In contrast, increased expression of genes linked to apoptosis and tumor suppression (*BAX, TNFRSF1A, GADD45GIP1, MAP3K5, TP53INP1, RAD23B, CCNB1, TK1* and *CYCS)* was characteristic of the sensitive cell lines. This was concordant with down-regulation of *ELF3, EFNA1, IRF9, TINF2, SEC22B, LEPRE1, LETMD1, DSTN, MAP2K5*, and *BNIP*, genes implicated in proliferation, survival, and metastasis (figs. S8B, C).

Consistent with the gene expression data, the zebularine-sensitive cell lines (Huh7, KMCH) showed a preferential demethylation of genes involved in tumor-suppressor activity, apoptosis, and cell-cycle regulation upon zebularine treatment, while in the resistant cell lines (WRL68, WITT) zebularine caused demethylation of tumor-promoting genes (*CTGF, MCF2, MME, NOS2A, TGFB2, S100A4, PTPRG, IGFBP5, DDR1*, and *CSPG2*) (table S2). Together, these data emphasize that zebularine may cause either oncogenic or pro-apoptotic effects, depending on the resistance or sensitivity of the liver cancer cell lines to zebularine.

Antitumor efficacy of zebularine therapy *in vivo*

To confirm the therapeutic potential of zebularine *in vivo*, several human xenograft models were evaluated. First, we showed that exposure to zebularine *in vitro* for 7 days prevented *in vivo* tumor growth of sensitive (Huh7, KMCH) HCC cell lines but was ineffective against the resistant (WRL68, WITT) cell lines growth in a model of subcutaneous (s.c.) transplantation in nude mice ($P<.002$) (fig. S4). To exclude influences of the recipient mouse strain, these findings were confirmed in a complementary analysis of s.c. transplantation of zebularine-treated Huh7 (sensitive) and WRL68 (resistant) cells (n=4–6/group) in immunodeficient NOD/SCID mice with a limited dilution analysis. The tumor initiating frequency (TIF) was reduced in sensitive ($P<.0001$) as compared to the resistant transplants (table S3).

As a final validation of antitumor efficacy of zebularine *in vivo*, we established an orthotopic xenograft model in SCID/Beige mice (fig. S9A). Mice received intrasplenic transplantation of luciferase-expressing HCC cells and subjected to bioluminescence imaging before initiation of zebularine therapy to ensure a comparable intrahepatic tumor burden between control and treatment groups (Figs. 2A, B). Zebularine was administered at the end of the second week when on average 50% of the total liver was comprised of tumor tissue (figs. S9B, C). To overcome low bioavailability and maintain therapeutically active concentrations of zebularine, we optimized the dosing scheme on the basis of pharmacokinetic data(16,33–34) (fig. S10A) and included raloxifene, an inhibitor of AOX1, a rate limiting enzyme in zebularine metabolism in the liver(35) (fig. S10B). The treatment caused no toxicity as judged by similar weights of mice before and after zebularine therapy (fig. S11). Addition of raloxifene at a dose optimized by allometric scaling (1mg/day) in combination with zebularine significantly augmented the anticancer potency of zebularine monotherapy as shown by a 7-time versus a 2.7-time reduction (P <.05) in total tumor bioluminescence at week two (Fig. 2B and figs. S10A and S12), decrease in liver-to-body weight ratio (P<.002) and improved histology (Fig. 2A–C). Furthermore, a detailed analysis of mice transplanted with Huh7^{luc+} cells expressing mCherry fluorescent protein revealed that the combined therapy also decreased the frequency and average size of pulmonary metastasis (P<.028) as demonstrated by bioluminescence imaging (Fig. 2D) and whole organ confocal microscopy (fig. S13). The treatment, however, was ineffective against brain metastasis (Fig. 2E). Consistent with the transcriptome and methylation data, the therapy markedly increased the overall survival of mice bearing liver tumors derived from the zebularine sensitive cancer cells (Huh7^{luc+}, Huh1^{luc+}, and KMCH^{luc+}) (Figs. 2F–H and fig. S14A–C). In contrast, the same treatment significantly (P<.0003) increased the tumor growth rate (fig. S14D) and decreased survival of mice bearing zebularine resistant WRL68^{luc+} xenografts (Fig. 2I).

To examine the molecular mechanisms underlying antitumor effects of zebularine and raloxifene therapy *in vivo*, we performed gene expression profiling of liver tumors from Huh7^{luc+} transplants treated either with raloxifene alone or zebularine and raloxifene combined. To detect early zebularine effects, individual Huh7-derived tumors were resected 3 days after completing the treatment and subjected to microarray analysis. 484 differentially expressed genes were identified by Bootstrap t-test (5,000 repetitions, P≤.01). Hierarchical clustering revealed two gene clusters that significantly separated tumors from control and zebularine-treated mice (Fig. 3A). Analysis of the functional gene connectivity demonstrated that beneficial effects of therapy were associated with a preferential down-regulation of key molecules controlling cancer cell proliferation coupled with an increased expression of the major initiator caspases (*CASP*2 and *CASP9*) involved in the activation of apoptosis (Figs. 3B, C).

The comparison of differentially expressed genes in response to zebularine treatment *in vivo* (Figs. 3B, C) and *in vitro* (fig. S8) revealed a significant overlap between the key networks. In sensitive cancer cell lines, zebularine-induced gene expression modulations caused inhibition of proliferation coupled with increased apoptosis, whereas zebularine-resistance was related to upregulation of key oncogenes. Together, these results show that epigenomic therapy with zebularine may produce differential molecular effects on liver tumor growth *in vitro* and in several experimental animal models, and that these effects may be therapeutically beneficial or may be detrimental.

Prognostic value of the zebularine response signatures

We developed a transcriptomic-based predictor of zebularine-sensitivity for human HCC. Integration of the zebularine response gene signature with primary HCCs from 57 patients analyzed on the NIH oligo-array platform stratified patients according to survival (Training

set). The prognostic power of the signature was validated in an independent data set of primary HCCs from 53 patients analyzed by Illumina bead chips (fig. S15).

An optimized gene classifier containing 70 genes was constructed from the zebularine response gene signature (table S4) and validated by NanoString multiplex target profiling (fig. S16). The accuracy of class prediction of the classifier by 7 different models ranged from 84 to 96% in both data sets, demonstrating its ability to predict clinical outcome of HCC patients. Multivariate analysis of the clinical variables demonstrated a statistically significant association between survival, invasion, grade, recurrence, and expression of c-MET and AFP (Table 1). The zebularine classifier was significantly enriched in (ES=0.5, $P<.002$) and positively correlated with subtype A HCC (Fig. 4A) as assessed by nonparametric gene set enrichment analysis(36). Furthermore, meta-analysis of publicly available gene expression and clinical data using the 70-gene classifier demonstrated its ability to predict clinical outcome for numerous types of human cancer ($P<.0001$, odds ratio >2) (Fig. 4E). A Cox proportional hazard model was then applied to test the prognostic utility of the zebularine classifier. Using Wald statistics, the classifier was reduced to 20 genes identified at the nominal threshold level $P<.01$ for each univariate test with at least a 2-time difference in expression ratio (Fig. 4B). These 20 genes were sufficient to correctly stratify HCC patients according to overall survival ($P<.002$) and disease recurrence ($P<.0009$) (Figs. 4C, D).

Next, the 133-gene zebularine demethylation signature (Fig. 1B) was shown to predict overall survival of HCC patients ($P<.02$) with and accuracy that ranged from 87 to 96% (fig. S17). To predict which HCC patients are likely to benefit from zebularine therapy, patients with poor clinical outcome (subtype A) and high methylation index(12) (fig. S1) were clustered with the 133-gene demethylation signature. Hierarchical clustering demonstrated the ability of the 133-gene signature to subdivide the subtype A HCC into two separate subclasses (0.90, $P<.0001$) (Figs. 5A–C). The zebularine resistant cell lines clustered with the high-risk hepatoblast-like (HB-type) HCC characterized by the worst prognosis as compared to hepatocyte-like (HC-type) HCC(6), suggesting that HB-type patients may be resistant to treatment whereas HC-type HCC patients are likely to benefit from zebularine therapy. Finally, using meta-analysis, we showed that the zebularine demethylation signature was predictive of drug-sensitivity in other cancer types (gastrointestinal, pancreatic, and leukemia) ($P<.0001$, odds ratio>2) (Fig. 5D), implying its broader clinical utility. In each incidence more than 25% of the signature was represented in the top 10% under-expressed genes.

DISCUSSION

Liver cancer is the fasted growing cancer in the United States, (37), and only 30% of the HCC patients are eligible for curative treatment (transplantation)(4). The multikinase inhibitor sorafenib is currently the only available drug for systemic therapy that provides survival benefit for advanced HCC patients(3). This has rendered HCC a major public health problem which is in need for both diagnostic markers and novel treatment strategies.

Here, we report a comprehensive preclinical characterization of gene expression alterations caused by epigenetic modulation in liver cancer cells by DNA demethylating agent zebularine. The work sheds new light on the functional and clinical implications of epigenetic modulation in liver cancer and identifies zebularine response gene and demethylation signatures predictive of clinical outcome in HCC patients as a new diagnostic and prognostic tool for selecting HCC patients who may benefit from epigenetic therapy.

A key finding in the study is the ability of the zebularine response gene and demethylation signatures to accurately predict clinical outcome of HCC patients. The effect of zebularine on gene expression and DNA methylation correlated with biological behavior *in vitro* and accurately predicted either beneficial or detrimental effects of zebularine *in vivo.* Despite a limited gene-to-gene overlap, a high degree of concordance was found in predicting the prognostic value of the zebularine response between gene expression and high-throughput DNA methylation profiling. A limited overlap between aberrant methylation and gene expression was also found in a recent large-scale genome-wide methylation study of patients with acute myeloid leukemia(38–39). The authors attributed the low correlation to DNA methylation-associated transcriptional repression which can vary dependent on the promoter.

When integrated genomics was applied to subclass A HCC (6), the anticipated target group for epigenetic therapy due to the highest degree of DNA CpG methylation, the patients with HC-type HCC in subclass A, were identified as the likely responders to epigenetic chemotherapy. Importantly, zebularine treatment resulted in either oncogenic or pro-apoptotic effects in resistant and sensitive liver cancer cell lines, respectively, demonstrating the critical role of correct selection of cancer patients for epigenetic treatment. Furthermore, independent validation of the predictive abilities of the 70-gene zebularine classifier by NanoString multiplex target profiling suggests that the latter could be effectively used as a diagnostic tool in a clinical setting as a step towards personalized medicine.

In conclusion, this study is the first proof-of-principle that therapeutic strategies designed to modify the methylation status of liver cancer cells may be beneficial for a subset of patients with advanced stage of HCC. The next challenge is to determine the molecular mechanism(s) driving zebularine sensitivity and resistance to achieve more effective targeting and clinical translation of epigenomic therapy in liver cancer.

MATERIALS AND METHODS

Cell culture and treatment

Human primary HCC cells (Celprogen) and liver cancer cell lines were grown in DMEM, supplemented with 2 mM L-glutamine, 1 unit/mL penicillin/streptomycin, and 10% FCS. Normal hepatocyte and cholangiocyte cell lines (THLE-3 and H69) were grown in BEGM (Lonza), supplemented with a BEGM bullet kit, 2 mM L-glutamine, 1 unit/mL penicillin/streptomycin, and 10% FCS. THLE-3 and H69 were grown in DMEM 24 h prior to analysis. Cholangiocarcinoma cell lines were purchased from RIKEN BRC Cell Bank (Koyadai, Japan). H69, KMCH, WITT and KMBC were a gift from Dr. G.J. Gores (MAYO Clinic, USA). Each cell line was treated with 100 or 200 μM zebularine (Drug Synthesis and Chemical Branch, Developmental Therapeutics Program, Division of Cancer Treatment and Diagnosis, NCI) for 7 days. Media and reagents were changed every 3 days.

Apoptosis assay

A total of 2×10^4 parental cells were grown in 8-well chamber slides (IBIDI), each in triplicates. After 24 h the cells were either treated with 100 μM zebularine, or medium was changed for the control wells. After 72 h, the medium was supplemented with 2 μg/ml Acridine-Orange (Sigma-Aldrich) and ethidium-bromide (Promega) and imaged by confocal microscopy (Zeiss NLO510) at 40X. In each well cells were counted in five microscope fields. We report all data as mean percentage apoptotic cells ± S.E.M.

FACS analysis

Each cell line was plated in T75 culture flasks at 1×10^6 cells 24 h prior to treatment with 100 μM zebularine. Cells were trypsinized after 72 h and fixed in ice-cold 70% EtOH. Washed cells were incubated with 50 μg/ml propidium iodide and 1 mg/ml RNase TypeIIA (Sigma) and 2.5×10^4 events were collected on a Calibur Flow cytometer (BD Bioscience) configured with CellQuest Pro software. Each assay was performed in triplicate. Data analysis was performed using FlowJo 7.2.4. We report all data as percentage mean accumulation in G2-phase ± S.E.M.

Cytotoxicity assay

The sensitivity of each cell line and the primary HCC cells to zebularine was measured with a colorimetric assay using WST-1 according to manufacturer's protocol (Roche Applied Sciences). The cells were plated at a density of 1×10^5 in 100 μL DMEM per well of a 96-well plate. After 24 h, the cells were treated with 100 μM zebularine and incubated for 72 h. Absorbance of WST-1 was measured at 450 nm for 0.5–4 h (M5, Molecular Devices). Cell viability was defined as the absorbance of the treatment group compared to the control group (n=4), calculated as percent mean change ± s.d.

Subcutaneous xenograph transplantation

Athymic $ncr^{nu/nu}$ (NCI-Frederick) female mice were injected subcutaneous on the neck with 1×106 cells and the formation of tumors was followed weekly using a vernier caliper. Huh7, WRL68, KMCH and WITT were subjected to mock or treatment with 100 or 200 μM zebularine and cultured for 7 days prior to transplantation (n=4/group). When a tumor reached 16–18 mm in diameter, mice were euthanized and the tumors excised and weighted. Tumor volumes were calculated according to, $V= 4/3\pi \times (\text{length}/2) \times (\text{width}/2) \times ((\text{length} + \text{width})/4)$.

Experimental design

After a recovery phase (day 8), transplanted mice were imaged and randomized into groups. The study design and dose was evaluated by simulations in ADAPT II (BMSR, USC). *Study 1:* A dose of 350 mg/kg zebularine dissolved in HBSS w/Ca^{2+}/Mg^{2+} was given per mouse at the following experimental procedure, 200 μL/mouse thrice daily for three days at an 8 h interval. The treatment group (n=5/group/week) was given the first dose in the morning of day 10. The control group (n=5/group/week) received 200 μL HBSS trice daily for three days. Following the dosing schedule, the animals were imaged twice weekly. *Study 2:* To prolong the exposure of zebularine *in vivo*, a once-daily administration of raloxifene (Sigma Aldrich) 1mg/mouse/day was selected with a study start two days prior to zebularine therapy. The required raloxifene dose was calculated using allometric scaling(40) according to Balfour *et al.*(41). Raloxifene was dissolved in 3% DMSO in faucet water. The body and liver weights were measured and the liver/body ratio was calculated. At euthanasia organs were collected and imaged *ex vivo* as a measure of metastases from the liver.

Bioluminescence imaging

Human hepatic cancer cell lines Huh1, Huh7, WRL68, and KMCH were stably transfected with $pGL4.17^{Luc+}$ vector (Promega) under the control of a β-actin promoter, and positive clones were selected using 400 μg/mL geneticin. Luciferase positive clones were selected by *in vitro* bioluminescence imaging using 2 mg/mL luciferin (Biosynth). For *in vivo* bioluminescence imaging luciferin was prepared by dissolving 15 mg/mL Dluciferin K^+-salt in phosphate buffered saline w/o Ca^{2+}/Mg^{2+} and sterile filter through a 0.22 μm syringe filter. Mice were anesthetized for 3 min with 5% isoflorane in oxygen, and kept at 2% isoflorane throughout the imaging procedure. Each mouse was injected intraperitoneal with

10 μL/g body weight luciferin and placed in the imaging IVIS100 chamber (Xenogen). Images were recorded 5 min after luciferin injection and reported as total flux (photons/sec). *Ex vivo* imaging was carried out on selected organs following *in vivo* bioluminescent imaging and resection. Imaging and analysis was performed using Living Image Software v3.0.

Orthotopic Liver Transplantation

6-week-old male SCID/Beige mice (Charles River) were anesthetized by inhalation of 5% isoflorane in oxygen. 0.5×10^6 cells in 50 μL phosphate-buffered saline were injected into the splenic pulp using a 27-gauge needle. Spleens were removed 30 sec after injection. Wounds were closed in two layers using 3-0 silk suture and surgical clips. Liver function was monitored by periodic blood collection via orbital plexus. Body weights were recorded before and after treatment, as a measure of drug toxicity. Liver weights were recorded at death. Animals were housed in an AAALAC facility and cared for in accordance with the guidelines from the Animal Care and Use Committee at the US National Cancer Institute, NIH. The overall survival probabilities were estimated according to the Kaplan-Meier method and Mantel-Cox statistics. All statistical analyses were performed using Mann-Whitney (two-tailed) test after evaluating the normality (D'Agostino & Pearson omnibus test) and variance (F-test).

Whole-organ confocal microscopy

SCID/Beige mice were transplanted intrasplenic using 0.5×10^6 Huh7$^{luc+/mCherry}$ cells. Surgery was performed as explained in detail in the methods section (Orthotopic liver transplantation). Lung and liver samples were obtained for confocal microscopy (Zeiss NLO710). The connective tissue (SHG, White) in the lung was imaged by 2-photon confocal microscopy (40X).

Limited dilution analysis

Transplantations were performed using Non-obese Diabetic/Severe Combined Immunodeficient (NOD/SCID) mice at 6 to 9 weeks of age. Cells were resuspended in DMEM and Matrigel (BD Bioscience) in a dilution of 1:1 before s.c inoculation into both flanks. Control injections with DMEM and Matrigel did not produce tumor growth. Tumor formation was monitored weekly by palpation over a period of 8 weeks. Limiting dilution analysis (LDA) was performed using (http://bioinf.wehi.edu.au/) and the tumor initiating cell frequency calculated for treated and untreated cells.

Microarray analysis

Total RNA was extracted from zebularine treated cell lines and 53 human HCC tissues (Qiagen). The HCC samples were obtained from patients undergoing partial hepatectomy as treatment for HCC(7,30). Tissue banking was approved by the Institutional Review Board of the US National Cancer Institute, NIH. The RNA integrity was estimated ($A_{260}/A_{280}>2$) by gel electrophoresis. 200 ng total RNA was amplified and incubated for 16 h at 37°C (Ambion). The efficiency of the cRNA amplification was quantified using the RiboGreen RNA kit (Invitrogen). Array hybridization, washing, Cy3-streptavidin labeling (GE Healthcare), and scanning was performed on a BeadStation 500 using reagents and protocols supplied by the manufacturer (Illumina). 750 ng biotinylated cRNA was hybridized to humanRef-8v2 beadchips for 18 h at 58°C. Image analysis and data extraction was automated using BeadScanv3.2.

Statistical analysis

Data collection was performed with BeadStudiov3.3. Each probe was randomly represented by an average of 30 replicates. Bead signals were computed with weighted averages of intensities, local background was subtracted, and the median absolute deviation was used to remove outliers(42–43). Detection *P* values were computed using a nonparametric model based on signals of the negative controls(44). A detection score was computed on the basis of the z value of a gene relative to the z value of the negative controls. Signals differing from the background with $P \leq .01$ were called. Data sets were normalized using quantile normalization with background subtraction. Technical error was estimated using iterative robust least squares fit. The false discovery rate was empirically estimated using the Benjamini-Hochberg procedure (45), considering background noise and sample variability (46). The condition array (n=3) for each cell line was analyzed individually using matched controls (n=3) as reference. Genes differentially expressed at $P \leq .001$ in either condition were filtered using 1-way ANOVA with GeneSpring GX7.3.1 (Agilent Technologies). Signatures for either HCC or CC cell lines were established, subtracting genes common to the corresponding normal control cell lines (THLE-3 or H69, respectively). The zebularine signature was generated by integrating the data sets following standardization using z-transformation. The probability of survival and recurrence were estimated according to the Kaplan-Meier method and Mantel-Cox statistics with Prismv5.01 (GraphPad). Multivariate statistical analysis ($\alpha=0.05$) with pair-wise correlation (JMP7, SAS). The pair-wise correlation ($\sigma=\pm1$) of clinical variables and their significance are given in Table 1.

To estimate the correct classification of drug-response, a Class Random Variance model using 7 different prediction algorithms, including compound covariate predictor, diagonal linear discriminator, 1-nearest neighbor, 3-nearest neighbors, nearest centroid, support vector machine, and Bayesian compound covariate, were used for class comparison to build the prediction model ($\alpha \leq .001$). To estimate the accuracy of the prediction model, random permutations during leave-one-out cross-validation were repeated 1,000 times (BRB-ArrayTools v3.8.0). A Cox proportional hazards model and Wald statistics were used to identify genes significantly associated with survival ($P \leq .01$). To estimate the accuracy, univariate permutation tests were repeated 10,000 times.

NanoString multiplex target profiling

CodeSets (Reporter and Capture probe sets) for the 70-gene zebularine classifier (table S4) were custom designed by NanoString. Briefly, 100 ng total RNA for each sample (n=3) was mixed with the supplied reagents according to the manufactures' description (NanoString Technologies) and hybridized at 65 °C over night. Next day, the samples were processed and analyzed using the nCounter Prep Station (NanoString Technologies). Data analysis was performed by first subtracting background noise (negative controls), adjusting the expression values according to positive control values, and normalizing the data set according to housekeeping genes. ΔCt values were calculated for each gene. The data set was standard normalized before integration with the Illumina data set.

Methylation array

Genomic DNA was extracted according to the manufacturer's protocol (Qiagen). DNA yield and quality were assessed by nanodrop (Thermo Scientific). 2 μg DNA were chemically modified by sodium bisulfite according to the manufacturer's protocol (Zymo Research) and the converted DNA was quantified using Quant-iT OliGreen ssDNA assay Kits (Invitrogen). Each sample was hybridized to GoldenGate methylation array(29) (Illumina). Allele extension, ligation, amplification and hybridization were performed according to the manufacturers' description. Imaging and data extraction were performed with BeadScanv3.2. Methylation data were analyzed in BeadStudiov3.2. The data were

normalized according to the background. An average of negative control signals were subtracted and probe signals given as β values(29). The β-value is reported between 0 (unmethylated) and 1 (methylated). Each bead type is represented with a 30-fold redundancy. Differentially methylated genes were identified using non-parametric multivariate permutations tests (BRB-ArrayTools v3.8.0). This test is robust, particularly when the number of samples within a class is small. Furthermore, it takes into account the correlation structure of the genes.

Validation

The HumanMethylation27 infinium methylation arrays cover 27.578 CpG loci (>14.000 genes). The arrays were hybridized using 200ng bisulfite converted genomic DNA according to the manufactures' description (Illumina). Briefly, the data was analyzed by GenomeStudio 2010 methylation module version 1.61 using the Illumina error model. The genes included in the zebularine demethylation signature was retrieved and analyzed according to description.

Supplementary Material

Refer to Web version on PubMed Central for supplementary material.

Abbreviations

CC	Cholangiocarcinoma
HB	Hepatoblast-like
HC	Hepatocyte
HCC	Hepatocellular carcinoma
LOOCV	Leave-one-out cross-validation
Ra	Raloxifene
Zebularine	1-(β-D-ribofuranosyl)-1,2-dihydropyrimidin-2-one

REFERENCES AND NOTES

1. Parkin DM, Bray F, Ferlay J, Pisani P. Global cancer statistics, 2002. CA Cancer J Clin. 2005; 55:74. [PubMed: 15761078]
2. Cheng AL, Kang YK, Chen Z, Tsao CJ, Qin S, Kim JS, Luo R, Feng J, Ye S, Yang TS, Xu J, Sun Y, Liang H, Liu J, Wang J, Tak WY, Pan H, Burock K, Zou J, Voliotis D, Guan Z. Efficacy and safety of sorafenib in patients in the Asia-Pacific region with advanced hepatocellular carcinoma: a phase III randomised, double-blind, placebo-controlled trial. Lancet Oncol. 2009; 10:25. [PubMed: 19095497]
3. Llovet JM, Ricci S, Mazzaferro V, Hilgard P, Gane E, Blanc JF, de Oliveira AC, Santoro A, Raoul JL, Forner A, Schwartz M, Porta C, Zeuzem S, Bolondi L, Greten TF, Galle PR, Seitz JF, Borbath I, Haussinger D, Giannaris T, Shan M, Moscovici M, Voliotis D, Bruix J. Sorafenib in advanced hepatocellular carcinoma. N Engl J Med. 2008; 359:378. [PubMed: 18650514]
4. Llovet JM, Burroughs A, Bruix J. Hepatocellular carcinoma. Lancet. 2003; 362:1907. [PubMed: 14667750]
5. Lee JS, Chu IS, Heo J, Calvisi DF, Sun Z, Roskams T, Durnez A, Demetris AJ, Thorgeirsson SS. Classification and prediction of survival in hepatocellular carcinoma by gene expression profiling. Hepatology. 2004; 40:667. [PubMed: 15349906]
6. Lee JS, Heo J, Libbrecht L, Chu IS, Kaposi-Novak P, Calvisi DF, Mikaelyan A, Roberts LR, Demetris AJ, Sun Z, Nevens F, Roskams T, Thorgeirsson SS. A novel prognostic subtype of human

hepatocellular carcinoma derived from hepatic progenitor cells. Nat Med. 2006; 12:410. [PubMed: 16532004]

7. Lee JS, Thorgeirsson SS. Genome-scale profiling of gene expression in hepatocellular carcinoma: classification, survival prediction, and identification of therapeutic targets. Gastroenterology. 2004; 127:S51. [PubMed: 15508103]
8. Villanueva A, Newell P, Chiang DY, Friedman SL, Llovet JM. Genomics and signaling pathways in hepatocellular carcinoma. Semin Liver Dis. 2007; 27:55. [PubMed: 17295177]
9. Villanueva A, Toffanin S, Llovet JM. Linking molecular classification of hepatocellular carcinoma and personalized medicine: preliminary steps. Curr Opin Oncol. 2008; 20:444. [PubMed: 18525342]
10. Feinberg AP. The epigenetics of cancer etiology. Semin Cancer Biol. 2004; 14:427. [PubMed: 15489135]
11. Feinberg AP, Tycko B. The history of cancer epigenetics. Nat Rev Cancer. 2004; 4:143. [PubMed: 14732866]
12. Calvisi DF, Ladu S, Gorden A, Farina M, Lee JS, Conner EA, Schroeder I, Factor VM, Thorgeirsson SS. Mechanistic and prognostic significance of aberrant methylation in the molecular pathogenesis of human hepatocellular carcinoma. J Clin Invest. 2007; 117:2713. [PubMed: 17717605]
13. Bird A. DNA methylation patterns and epigenetic memory. Genes Dev. 2002; 16:6. [PubMed: 11782440]
14. Issa JP. DNA methylation as a therapeutic target in cancer. Clin Cancer Res. 2007; 13:1634. [PubMed: 17363514]
15. Yoo CB, Jones PA. Epigenetic therapy of cancer: past, present and future. Nat Rev Drug Discov. 2006; 5:37. [PubMed: 16485345]
16. Dote H, Cerna D, Burgan WE, Carter DJ, Cerra MA, Hollingshead MG, Camphausen K, Tofilon PJ. Enhancement of in vitro and in vivo tumor cell radiosensitivity by the DNA methylation inhibitor zebularine. Clin Cancer Res. 2005; 11:4571. [PubMed: 15958643]
17. Issa JP, Kantarjian HM. Targeting DNA methylation. Clin Cancer Res. 2009; 15:3938. [PubMed: 19509174]
18. Neureiter D, Zopf S, Leu T, Dietze O, Hauser-Kronberger C, Hahn EG, Herold C, Ocker M. Apoptosis, proliferation and differentiation patterns are influenced by Zebularine and SAHA in pancreatic cancer models. Scand J Gastroenterol. 2007; 42:103. [PubMed: 17190770]
19. Pinto A, Zagonel V. 5-Aza-2'-deoxycytidine (Decitabine) and 5-azacytidine in the treatment of acute myeloid leukemias and myelodysplastic syndromes: past, present and future trends. Leukemia. 1993 Suppl 1:51. [PubMed: 7683358]
20. Schwartsmann G, Schunemann H, Gorini CN, Filho AF, Garbino C, Sabini G, Muse I, DiLeone L, Mans DR. A phase I trial of cisplatin plus decitabine, a new DNA-hypomethylating agent, in patients with advanced solid tumors and a follow-up early phase II evaluation in patients with inoperable non-small cell lung cancer. Invest New Drugs. 2000; 18:83. [PubMed: 10830142]
21. Cheng JC, Yoo CB, Weisenberger DJ, Chuang J, Wozniak C, Liang G, Marquez VE, Greer S, Orntoft TF, Thykjaer T, Jones PA. Preferential response of cancer cells to zebularine. Cancer Cell. 2004; 6:151. [PubMed: 15324698]
22. Cheng JC, Matsen CB, Gonzales FA, Ye W, Greer S, Marquez VE, Jones PA, Selker EU. Inhibition of DNA methylation and reactivation of silenced genes by zebularine. J Natl Cancer Inst. 2003; 95:399. [PubMed: 12618505]
23. Yoo CB, Cheng JC, Jones PA. Zebularine: a new drug for epigenetic therapy. Biochem Soc Trans. 2004; 32:910. [PubMed: 15506921]
24. Cheng JC, Weisenberger DJ, Gonzales FA, Liang G, Xu GL, Hu YG, Marquez VE, Jones PA. Continuous zebularine treatment effectively sustains demethylation in human bladder cancer cells. Mol Cell Biol. 2004; 24:1270. [PubMed: 14729971]
25. Marquez VE, Eritja R, Kelley JA, Vanbemmel D, Christman JK. Potent inhibition of Hhal DNA methylase by the aglycon of 2-(1H)-pyrimidinone riboside (zebularine) at the GCGC recognition domain. Ann N Y Acad Sci. 2003; 1002:154. [PubMed: 14751833]

26. van Bemmel DM, Brank AS, Eritja R, Marquez VE, Christman JK. DNA (Cytosine-C5) methyltransferase inhibition by oligodeoxyribonucleotides containing 2-(1H)-pyrimidinone (zebularine aglycon) at the enzymatic target site. Biochem Pharmacol. 2009; 78:633. [PubMed: 19467223]
27. Feinberg AP, Ohlsson R, Henikoff S. The epigenetic progenitor origin of human cancer. Nat Rev Genet. 2006; 7:21. [PubMed: 16369569]
28. Bibikova M, Chudin E, Wu B, Zhou L, Garcia EW, Liu Y, Shin S, Plaia TW, Auerbach JM, Arking DE, Gonzalez R, Crook J, Davidson B, Schulz TC, Robins A, Khanna A, Sartipy P, Hyllner J, Vanguri P, Savant-Bhonsale S, Smith AK, Chakravarti A, Maitra A, Rao M, Barker DL, Loring JF, Fan JB. Human embryonic stem cells have a unique epigenetic signature. Genome Res. 2006; 16:1075. [PubMed: 16899657]
29. Bibikova M, Lin Z, Zhou L, Chudin E, Garcia EW, Wu B, Doucet D, Thomas NJ, Wang Y, Vollmer E, Goldmann T, Seifart C, Jiang W, Barker DL, Chee MS, Floros J, Fan JB. High-throughput DNA methylation profiling using universal bead arrays. Genome Res. 2006; 16:383. [PubMed: 16449502]
30. Andersen JB, Loi R, Perra A, Factor VM, Ledda-Columbano GM, Columbano A, Thorgeirsson SS. Progenitor-derived hepatocellular carcinoma model in the rat. Hepatology. 2010; 51:1401. [PubMed: 20054870]
31. Gardiner-Garden M, Frommer M. CpG islands in vertebrate genomes. J Mol Biol. 1987; 196:261. [PubMed: 3656447]
32. Takai D, Jones PA. Comprehensive analysis of CpG islands in human chromosomes 21 and 22. Proc Natl Acad Sci U S A. 2002; 99:3740. [PubMed: 11891299]
33. Beumer JH, Joseph E, Egorin MJ, Parker RS, D'Argenio D Z, Covey JM, Eiseman JL. A mass balance and disposition study of the DNA methyltransferase inhibitor zebularine (NSC 309132) and three of its metabolites in mice. Clin Cancer Res. 2006; 12:5826. [PubMed: 17020990]
34. Holleran JL, Parise RA, Joseph E, Eiseman JL, Covey JM, Glaze ER, Lyubimov AV, Chen YF, D'Argenio DZ, Egorin MJ. Plasma pharmacokinetics, oral bioavailability, and interspecies scaling of the DNA methyltransferase inhibitor, zebularine. Clin Cancer Res. 2005; 11:3862. [PubMed: 15897587]
35. Klecker RW, Cysyk RL, Collins JM. Zebularine metabolism by aldehyde oxidase in hepatic cytosol from humans, monkeys, dogs, rats, and mice: influence of sex and inhibitors. Bioorg Med Chem. 2006; 14:62. [PubMed: 16143537]
36. Mootha VK, Lindgren CM, Eriksson KF, Subramanian A, Sihag S, Lehar J, Puigserver P, Carlsson E, Ridderstrale M, Laurila E, Houstis N, Daly MJ, Patterson N, Mesirov JP, Golub TR, Tamayo P, Spiegelman B, Lander ES, Hirschhorn JN, Altshuler D, Groop LC. PGC-1alpha-responsive genes involved in oxidative phosphorylation are coordinately downregulated in human diabetes. Nat Genet. 2003; 34:267. [PubMed: 12808457]
37. El-Serag HB, Rudolph KL. Hepatocellular carcinoma: epidemiology and molecular carcinogenesis. Gastroenterology. 2007; 132:2557. [PubMed: 17570226]
38. Bullinger L, Armstrong SA. HELP for AML: methylation profiling opens new avenues. Cancer Cell. 2010; 17:1. [PubMed: 20129241]
39. Figueroa ME, Lugthart S, Li Y, Erpelinck-Verschueren C, Deng X, Christos PJ, Schifano E, Booth J, van Putten W, Skrabanek L, Campagne F, Mazumdar M, Greally JM, Valk PJ, Lowenberg B, Delwel R, Melnick A. DNA methylation signatures identify biologically distinct subtypes in acute myeloid leukemia. Cancer Cell. 2010; 17:13. [PubMed: 20060365]
40. West GB, Brown JH, Enquist BJ. A general model for the origin of allometric scaling laws in biology. Science. 1997; 276:122. [PubMed: 9082983]
41. Balfour JA, Goa KL. Raloxifene. Drugs Aging. 1998; 12:335. [PubMed: 9571395]
42. Galinsky VL. Automatic registration of microarray images. II. Hexagonal grid. Bioinformatics. 2003; 19:1832. [PubMed: 14512355]
43. Kuhn K, Baker SC, Chudin E, Lieu MH, Oeser S, Bennett H, Rigault P, Barker D, McDaniel TK, Chee MS. A novel, high-performance random array platform for quantitative gene expression profiling. Genome Res. 2004; 14:2347. [PubMed: 15520296]

44. Fan JB, Yeakley JM, Bibikova M, Chudin E, Wickham E, Chen J, Doucet D, Rigault P, Zhang B, Shen R, McBride C, Li HR, Fu XD, Oliphant A, Barker DL, Chee MS. A versatile assay for high-throughput gene expression profiling on universal array matrices. Genome Res. 2004; 14:878. [PubMed: 15123585]

45. Benjamini, Y YH. Controlling the False Discovery Rate: A Practical and Powerful Approach to Multiple Testing. Journal of the Royal Statistical Society. Series B (Methodological). 1995; 57:289.

46. Chudin E, Kruglyak S, Baker SC, Oeser S, Barker D, McDaniel TK. A model of technical variation of microarray signals. J Comput Biol. 2006; 13:996. [PubMed: 16761924]

47. **Acknowledgment**: We thank Dr. Divya Menon-Andersen for advice concerning zebularine pharmacokinetics, and Dr. Joseph W. Grisham for histopathological examination. We are grateful to Susan Garfield and Langston Lim for assistance with confocal microscopy, Dr. Agnes Holczbauer for providing mCherry expressing lentivirus, and Arthur Olson for proofreading the manuscript. **Funding**: Supported by the Intramural Research Program of the NIH, National Cancer Institute, Center for Cancer Research. **Author contributions**: J.B.A., V.M.F., J.U.M., C.R. performed all experiments; S.S.T. provided funding; J.B.A., V.M.F., S.S.T. wrote the paper; E.A.C., Y.H.L., D.S. provided materials/tools. **Competing interests**: The authors declare that they have no competing interests. **Array submission**: Microarray data was submitted to GEO http://www.ncbi.nlm.nih.gov/geo/query/acc.cgi?acc=GSE23991

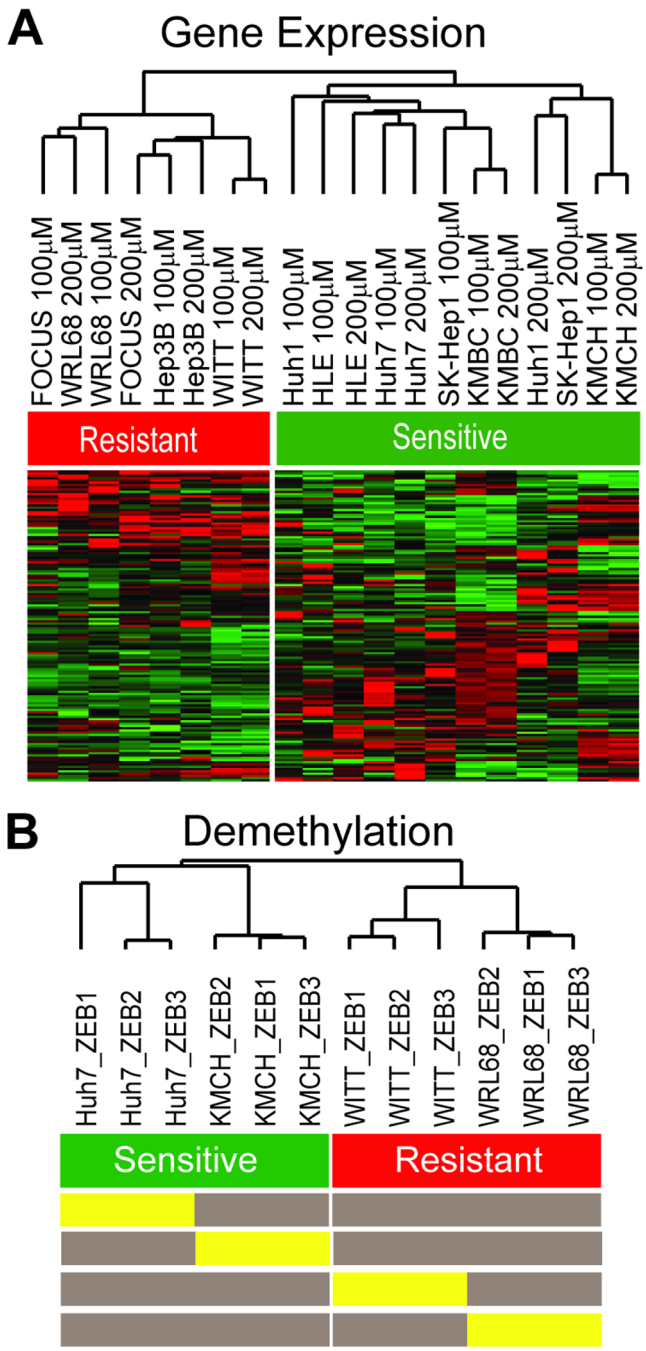

Figure 1.

Development of the zebularine response gene signature. (**A**) Unsupervised hierarchical clustering of gene expression data using the 323-gene zebularine response signature. The zebularine signature was derived from the gene lists of differential expressed genes computed at $P \leq .001$ for each individual cell line using a corresponding control sample as a reference. The signature included a total of 631 genes universally changed by zebularine in HCC and 451 genes in CC cell lines. Comparison of the gene lists with those in the corresponding non-tumorigenic cell lines identified gene expression changes which were unique to either HCC (238 genes) or CC cell lines (85 genes). Integration and clustering of the signature grouped the cell lines into two clusters, resistant (red, non-responder) and

sensitive (green, responder) depending on the zebularine-sensitivity. (**B**) Methylation profiling of cell lines treated with zebularine. A list of 133 demethylated genes ($P \leq .01$, $\Delta\beta \geq 0.17$) was identified by computing signatures for each cell line using a corresponding untreated sample as a reference (table S2). Note, that the cell lines clustered according to zebularine-sensitivity and corresponding xenographs response to zebularine therapy.

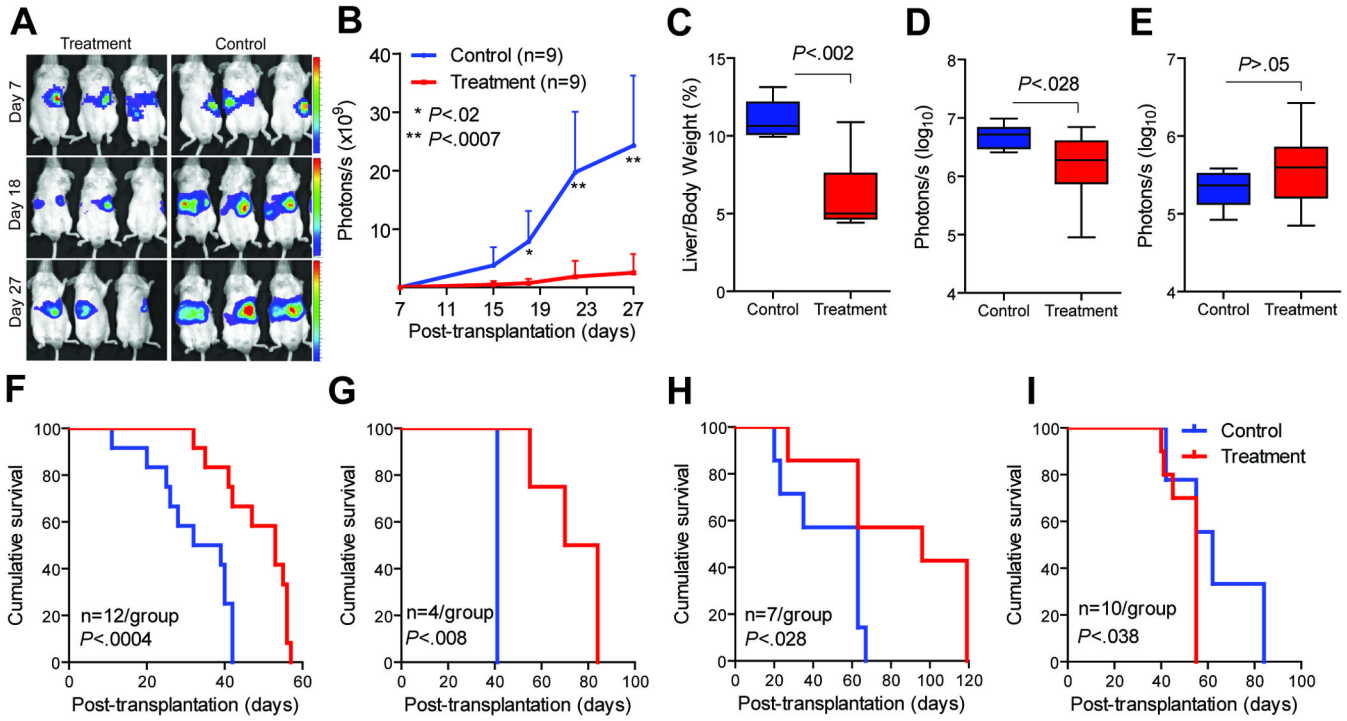

Figure 2.

Evaluation of the efficacy of the zebularine therapy *in vivo*. (**A**) *In vivo* bioluminescence imaging of Huh7^{luc+}-xenografts. Tumor bearing mice were randomly assigned either to control (raloxifene, n=9) or treatment (zebularine and raloxifene, n=9) based on the intensity of bioluminescence before zebularine and raloxifene therapy (day 9). Representative images at day 7, 18, and 27 are shown. (**A**) Quantification of bioluminescence. The total flux is plotted as photon/s (**C**) Liver/body weight. (**D**) Pulmonary metastases. Treated mice (red bar) developed less lung metastases as compared to controls (blue bar). The isolated lungs were reimaged *ex vivo* and total flux was plotted as photon/s ($\log_{10}$ scale). (**E**) Brain metastasis did not respond to therapy. The isolated brains were reimaged *ex vivo* and the total photon flux was reported as photon/s ($\log_{10}$ scale). (**F**) Survival analysis for Huh7^{luc+}-recipients representing a separate experiment. Kaplan-Meier plot and Mantel Cox statistics demonstrate that the reduction in tumor growth was associated with increased overall survival. (**G–I**) The overall survival of Huh1^{luc+}- (**G**), KMCH^{luc+}- (**H**) and WRL68^{luc+}-recipients (**I**), following zebularine therapy. Note, either beneficial (**G, H**) or inferior (**I**) effects of zebularine therapy on survival of tumor-bearing mice. Bars represent the mean ±s.d. Statistical significance was determined by Mann Whitney test (two-tailed).

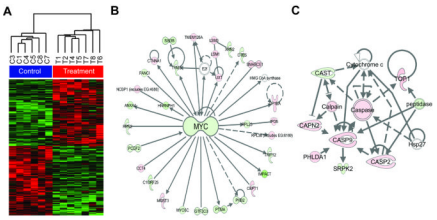

Figure 3.

Gene expression changes in response to zebularine therapy *in vivo*. (**A**) Hierarchical cluster analysis of liver tumors derived from the zebularine sensitive Huh7^{luc+}-xenografts identifies a list of 484 differentially expressed genes by Bootstrap-t ($P \leq .01$, 5,000 repetitions). Control tumors, raloxifene alone (n=6), and the treatment group zebularine and raloxifene (n=7). (**B, C**) Ingenuity Pathway Analysis shows zebularine and raloxifene treatment caused a preferential deregulation of genes controlled by the oncogene *MYC* (**B**) and up-regulation of initiator caspases (e.g. *CASP2* and *CASP9*) (**C**).

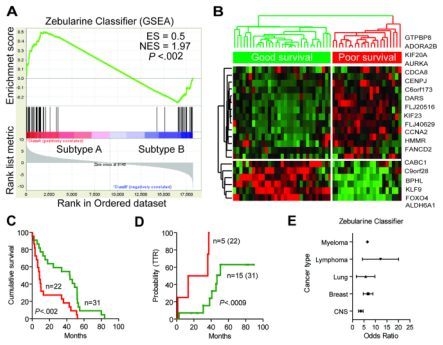

Figure 4.

Prognostic survival genes. (**A**) Gene Set Enrichment Analysis (GESA) of the zebularine classifier. Analysis of the classifier revealed an Enrichment Score (ES) of the rank-ordered genes which demonstrated a significant positive correlation with the poor survival subtype A HCC. (**B**) Hierarchical cluster analysis of the validation data set. Genes which were significantly ($P \leq .01$) associated with the disease outcome were identified by applying a Cox proportional hazards model and Wald statistics. 20 genes independently demonstrated a prognostic ability, based on the improved overall survival (**C**) and time to recurrence (**D**). Kaplan-Meier and Mantel-Cox statistics were used to determine levels of significance. (**E**) Meta-analysis using the zebularine classifier. The zebularine classifier is significantly associated to a study with a clinical outcome if the odds ratio >2, $P < .0001$ (Oncomine). Forest plot represent the odds ratio ± 95% CI.

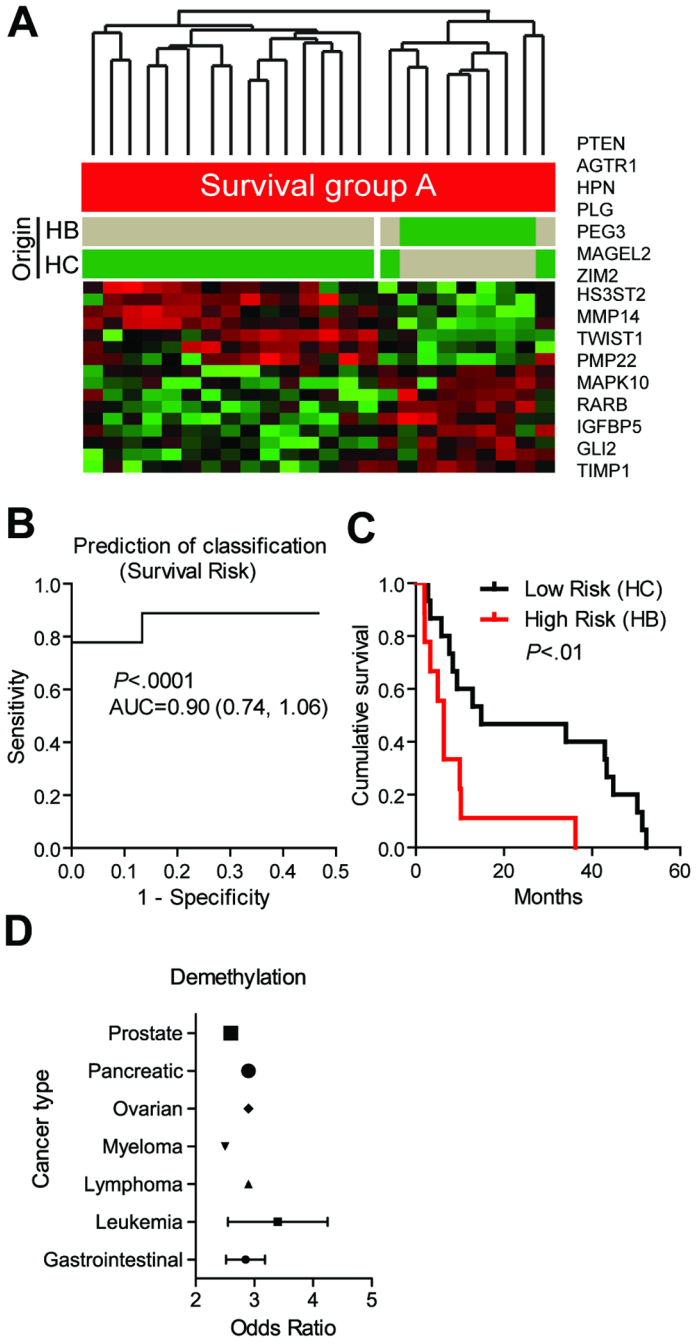

Figure 5.

Prediction of drug response. (**A**) Unsupervised clustering of subtype A HCCs based on the demethylation signature. The 133-gene list was significantly reduced to 16 genes which correctly predicted the classification using 7 different algorithms. (**B**) Sensitivity of the gene list to correctly predict the classification of patients within subtype A. The specificity is represented by the area under the receiver operating characteristic (ROC) curve (AUC, 95% CI) using Bayesian Compound Covariate prediction modeling during leave-one-out cross-validation. (**C**) Kaplan-Meier curves for survival risk prediction within subtype A HCC. Permutation p-value of the log-rank test statistic between risk groups was based on 100 permutations. (**D**) Meta-analysis using the demethylation signature. The signature is

significantly associated to a study if the odds ratio>2, $P<.0001$ (Oncomine). In each incidence >25% of genes in the signature is represented in the top 10% under-expressed genes (responders) within the gene set analyzed. Forest plot represent the odds ratio ± 95% CI.

Table 1

Clinical and pathological variables

Univariate*	**Events**		***P* value**
Survival	53		0.01
Tumor size (mm)	53		0.11
Grade 2	17		0.32
3	35		0.21
4	1		
Recurrence	53		0.27
Invasion	11		0.20
Vascularization	24		0.44
HBsAG	46		6.27E-6
Cirrhosis	53		0.82
MET (IHC)	53		8.23E-6
AFP (>300ng)	50		0.02
HB vs HC	53		0.002
A vs B	53		6.77E-10
Multivariate#	**Events**	**σ value**	***P* value**
Survival vs. MET	44	− 0.32	0.04
Survival vs. recurrence	44	0.87	< 0.0001
Invasion vs. grade	11	1.0	< 0.0001
Invasion vs. vascularization	11	0.84	0.001
Grade vs. size (mm)	53	0.30	0.03
Cirrhosis vs. size (mm)	53	− 0.32	0.02
HBsAG vs. AFP	45	0.49	0.0007
HBsAG vs. MET	46	0.78	< 0.0001
AFP vs. MET	50	0.41	0.003

#Multivariate analysis: *P* values given for a pair-wise correlation (σ).

*Chi-squared (χ^2) test.